LA-UR-86-2951



Los Alamos National Laboratory is operated by the University of California for the United States Department of Energy under contract W-7405-ENG-36



TITLE **BENDING AND FOCUSING EFFECTS IN AN FEL OSCILLATOR II NUMERICAL SIMULATIONS**

LA-UR--86-2951

DE86 015315

AUTHOR(S) **Brian D. McVey**
**Roger W. Warren**

SUBMITTED TO **To be presented at the Eighth Internation Free-Electron Laser Conference in Glasgow, Scotland, Sept. 1-5, 1986**

## DISCLAIMER



Los Alamos Los Alamos National Laboratory
Los Alamos, New Mexico 87545

# BENDING AND FOCUSING EFFECTS IN AN FEL OSCILLATOR II NUMERICAL SIMULATIONS *

B. D. McVey and R. W. Warren
Los Alamos National Laboratory
Los Alamos, NM 87545 USA

## ABSTRACT

Bending and focusing of the optical beam by the electron beam is investigated for an FEL oscillator configuration. Numerical calculations are performed with the simulation code, FELEX.

## I. INTRODUCTION

The free-electron laser interaction results in both a gain and a phase shift of the optical field[1]. In an FEL oscillator, the phase shift manifests itself in bending and focusing of the optical beam relative to the optical axis. Bending and focusing effects are the topic of this paper. As discussed in part I of this work[2], (hereafter referred to as I), bending and tilt of the optical beam were observed experimentally in the Los Alamos FEL experiment[2]. The observations were made when there was a misalignment between the electron beam and the optical beam axis. This suggested the electron beam had a prism effect on the optical beam. These physics considerations also predicted a focusing of the optical beam when there was alignment with the electron beam. The electron beam was both a gain media and could be modelled as a lens. We investigate these models in more detail by using the FEL oscillator simulation code FELEX[3]. In section II, we evaluate the effective index of refraction of the electron beam, and discuss its characteristics. In section III, we observe bending and focusing effects in a simulation of an FEL oscillator with parameters characteristic of the Los Alamos ERX experiment. In section IV, we discuss our results.

---

*Work performed under the auspices of the U. S. Department of Energy and supported by the Department of Defense U. S. Army Strategic Defense Command.

## II. THE EFFECTIVE REFRACTIVE INDEX

In this and the following section, we present results from the three-dimensional FEL simulation code, FELEX. The code has been described in detail elsewhere[7]. Relevant to the topic of this paper, the simulation code models the self-consistent interaction between the electron beam and the optical field. At the end of the wiggler, the optical field is then propagated through a resonant cavity back to the wiggler entrance where the FEL interaction is reinitiated. The optical properties of the electron beam can be characterized by a complex refractive index[4],

$$\eta_r - 1 = \frac{2\pi}{c} J \frac{a_w}{K_o E_o} F_u \frac{\cos(\psi + \theta_o)}{\gamma} \qquad (1)$$

$$\eta_i = -\frac{2\pi}{c} J \frac{a_w}{K_o E_o} F_u \frac{\sin(\psi + \theta_o)}{\gamma} \qquad (2)$$

where J is the current density, $a_w = e B_w/(mc^2 K_w)$, $E_o$ and $\theta_o$ are the optical field strength and phase, $K_o$ is optical wave number, and $F_u$ is the difference of Bessel functions. The energy of the electron is $\gamma mc^2$ and the phase of the electron in the optical wave is $\psi$. The brackets indicate an average over the electron distribution. A few observations can be made from the refractive index formula. Both the gain ($\eta_i$) and the additional phase shift ($\eta_r$) are dependent upon bunching of the electron beam (non-zero valves for the sin and cosine terms). Examples of the evolution of this electron bunching process along the length of the wiggler is seen in Figures 1a and 1b. Figures 1a and 1b are for the small signal regime, $I_{in} = 10^7 w/cm^2$, and for the saturated regime, $I_{in} = 10^{10} w/cm^2$. At saturation, the gain ($\eta_i$) is much lower, G = 2.5 percent, compared to G = 100 percent for Figure 3a. For both signal levels, the average value of $\eta_r$ is approximately the same but the variation, or electron bunching along the length of the wiggler is quite

different. Further the radial variation of $n_r$ is quite different for the two signal levels. The gain and refractive properties of the electron beam are seen to be nonlinear functions of the optical field strength.

We first estimate the magnitude of the bending and focusing by performing single pass simulations, and observing the bend and focusing in the output optical wave. The electron beam and optical beam parameters are listed in Table I. The electron beam profile is assumed to be Guassian, and the width of the electron beam is approximately one half the width of the Guassian optical mode. The waist of the initial optical mode was assumed to be at the center of the wiggler. For an aligned system, the effective focal strength of the electron beam may be estimated from the curvature of the optical beam in the far field. The curvature was found to be less than the vacuum propagation case, indicating that the waist moved from the center toward the end of the wiggler. For the electron beam parameters of Table I, the effective focal length of the lens at the center of the wiggler was 1140 cm.

In the set of simulations, next, the axis of the initial optical beam was translated a distance $\Delta y$ from the electron beam axis. The resultant bend angle $\lambda(I)$ defined as of the optical beam is plotted in Fig 2a as a function of $\Delta y$. The bend angle increases almost linearly with displacement and then saturates when the displacement equals the radius of the electron beam The bend angle is larger than would be predicted from a lens of the focal strength calculated for the aligned case. The reason for this is illustrated in Fig 2b where radial profiles of $n_r$-1 are plotted for three displacements of the optical beam. The refractive index or bending power is dependent upon the location of center of the optical field. The refractive index tends to follow but lag behind the displacement of the optical beam. The effective lens that models the electron beam is clearly a nonlinear medium.

## III. FEL OSCILLATOR SIMULATIONS

In this section, we describe simulation results for an FEL oscillator with parameters summarized in Table 1. Computer runs were made to simulate the

start-up of the FEL oscillator from the small signal regime to the saturated state. For the parameters of Table 1, the signal reached saturation in about 50 passes and the electron beam was turned off, after 120 passes. The optical signal then freely decayed. Three sets of simulations were performed. The first two illustrate the bending or refractive properties of the electron beam and the last the focusing power of the beam. In the first set, the optical axis was translated from the electron beam axis, and in the second set, the electron beam current was varied for a fixed optical axis displacement of .6 mm. The final set was a variation of electron beam current for a perfectly aligned electron beam and optical axis.

The walking mode oscillations (described in part I) are readily observed in the simulations for a misaligned system. The oscillations are observed in most diagnostics, of which Figure 3 is typical. In Figure 3 the centroid of the optical beam on the right mirror is plotted as a function of pass number. When the electron beam is turned off (pass number = 121), the optical beam oscillates about the optical axis with a characteristic frequency consistent with the ray tracing analysis of (I). Both tilt and and centroid displacement are larger in the small signal regime (before pass number 30) than in the saturated regime (pass numbers 60-120). The oscillations in the small signal regime are due to the fact that the initial starting conditions of the optical field (which match the empty cavity solution) are not an equilibrium solution when the electron beam is present.

Figures 4a and 4b plot the bend and tilt angles as defined in Figure 2 of (I) as a function of the displacement of the optical axis. Figure 4a is for the small signal regime, and Figure 4b is for the saturated state. An immediate observation is that the bend angles are comparable, but the tilt angles are quite different for the two signal levels. We attribute the larger tilt in the small signal regime to higher gain (~100 percent) compared to a gain of 2.5 percent at saturation. This is also illustrated in the refractive index plots of Figures 1a and 1b. For displacements of the optical axis greater than .6 mm

higher order optical modes (TEM01) develop, and the optical field solution has two peaks. Generation of higher order modes is observed when the optical axis displacement is comparable to the size (1/e point) of the electron beam. We note that a simulation for .6 mm optical axis displacement with $\eta_r$-1 set equal to zero showed a tilt angle of approximately one half of the value in Fig. 4 and a bend angle of zero.

Figures 5a and 5b illustrate the bend and tilt angles as a function of electron beam current for a fixed optical axis displacement of .6 mm. In the small signal regime, 5a, the tilt angle increases along with an increase in gain, however the bend angle remains nearly constant and then decreases. At saturation, 5b, the bend angle increases with current and the tilt angle remains nearly constant. For currents greater than 250 A, the optical field is unstable to higher order mode generation.

In the last set of simulations, we investigate focusing of the electron beam for a perfectly aligned system. Breathing mode oscillations are observed in the simulations as seen in Figure 6. The width of the optical beam on the right mirror is seen to oscillate at twice the frequency of the walking mode of Figure 3. The optical mode size in the presence of the electron beam is smaller than the empty cavity case which is indicative of focusing of the electron beam. An estimate of the focal power of the electron beam observed in the simulations can be made by comparing the radius of curvature of the beam on pass 120 to that on pass 121. The comparison is made in the far field and pass 120 is the last pass with the electron beam present. The estimate places a lens of focal power f at the geometric center of the resonant cavity which is the waist of the optical beam. The difference in far field curvatures with an without the lens is equal to the change in the position of the optical waist, $L = R_{121} - R_{120}$. From Gaussian optics, $L \simeq z_r^2/f$, so we obtain the formula for the focal power of the lens.

$$f = \frac{z_r^2}{R_{121}-R_{120}} \qquad (3)$$

Figure 7 illustrates the effective focal strength, $\frac{1}{f}$, of the electron beam as defined by Eq. 3 as a function of current for small signal and for saturation where the gain is fixed at 2.5 percent. It is observed that the focal length tends to flatten out at larger currents and, for small signal, approaches the stability limit. This flattening is probably due to an ~~increased~~ greater number of synchrotron oscillations due to longer optical interaction as the current is increased. The refractive index oscillates as in Figure 3b which was at 150 A and shows one synchrotron oscillation.

## IV. DISCUSSION OF RESULTS

In the context of numerical simulations and corroborated by experiment (~~part~~ I), we have shown that an electron beam can bend and focus an optical beam. The underlying physics involved is identical to that of optical guiding by an elongated high current electron beam[4,5]. The bending angle is toward the electron beam axis indicating a guiding effect. In an FEL oscillator, the guiding of the electron beam is balanced by the requirement that the optical beam be aligned with the optical axis. In the simulations, we have ob served an instability boundary for the TEMoo mode. For a given current, an increasing displacement of the optical axis will generate the TEMol mode. For a given misalignment, higher currents will be unstable to higher order mode generation. The boundaries are indicated in Figures 4 and 5, and at even higher currents (1000A) the displacement boundary is moved in to .3 mm. The bounded volume of parameter space for the TEMoo mode will probably decrease in concentric and confocal resonators, and we have observed a decrease when the output coupling is increased above the 2.5 percent assumed here.

## REFERENCES


[1] W. B. Colson and S. K. Ride, Physics of Quantum Electronics, Vol. 5, eds. s. F. Jacobs, M. Sargent and M. O. Scully (Addison-Wesley, Reading MA, 1978) p. 157.

[2] B. E. Newnam, et al., IEEE J. Quant. Electron., QW-21, (1985), P. 867.

[3] B. D. McVey, Proc. of the Lake Tahoe FEL Workshop, to be published

[4] E. T. Charlemann, A. M. Sessler, and J. S. Wurtele, Phys. Rev. Lett. 54, (1985) p. 1925.

[5] G. T. Moore, in Proceedings of the International Workshop on Coherent and Collective Properties of Electron and Electron Radiation, Como, Italy, 1984 Nucl. Instrum. Methods in Physics.

TABLE I

| | |
|---|---|
| Electron beam: | $\gamma = 42.55$, $I = 150$ A, $\epsilon = 6.3 \times 10^{-4}$ cm-rad |
| | $r_y(o) = .8$ mm, $r_x(0) = 1.0$ mm, $r_x(L_w/2) = 1.4$ mm |
| Wiggler: | uniform, $L_w = 100$ cm, $\lambda_w = 2.73$ cm |
| | $B_w = 3000$ G |
| Optical: | $\lambda = 10$ μm, $Z_r = 50$ cm, $w_o = 1.2$ mm, |
| | $w(L_w/2) = 1.8$ mm |
| Optical Cavity: | stability factor = .93 |
| | mirror positions: $Z_1 = -351.9$ cm, $Z_2 = 339.93$ cm |
| | mirror curvatures: $R_1 = R_2 = 353$ cm |

## FIGURE CAPTIONS

Fig. 1 Refractive index along the wiggler axis, a) small signal, b) large signal.

Fig. 2 a) Bend angle as a function of optical axis displacement, b) refractive index variation for three displacements of the optical axis.

Fig. 3 Optical centroid on the right hand mirror during start-up and decay (walking mode oscillation) of the FEL oscillator.

Fig. 4 For the oscillator, bend and tilt angles as a function of optical axis displacement for I = 150 A, a) small signal b) large signal.

Fig. 5 For the oscillator, bend and tilt angles as a function of electron current for $\Delta y$ = .6 mm, a) small signal, b) large signal.

Fig. 6 Optical width on the right hand mirror during start-up and decay (breathing mode oscillation) of the FEL oscillator.

Fig. 7 Focusing power $1/f$, of the electron beam for an aligned system at small signal and saturation.

Fig. 1a

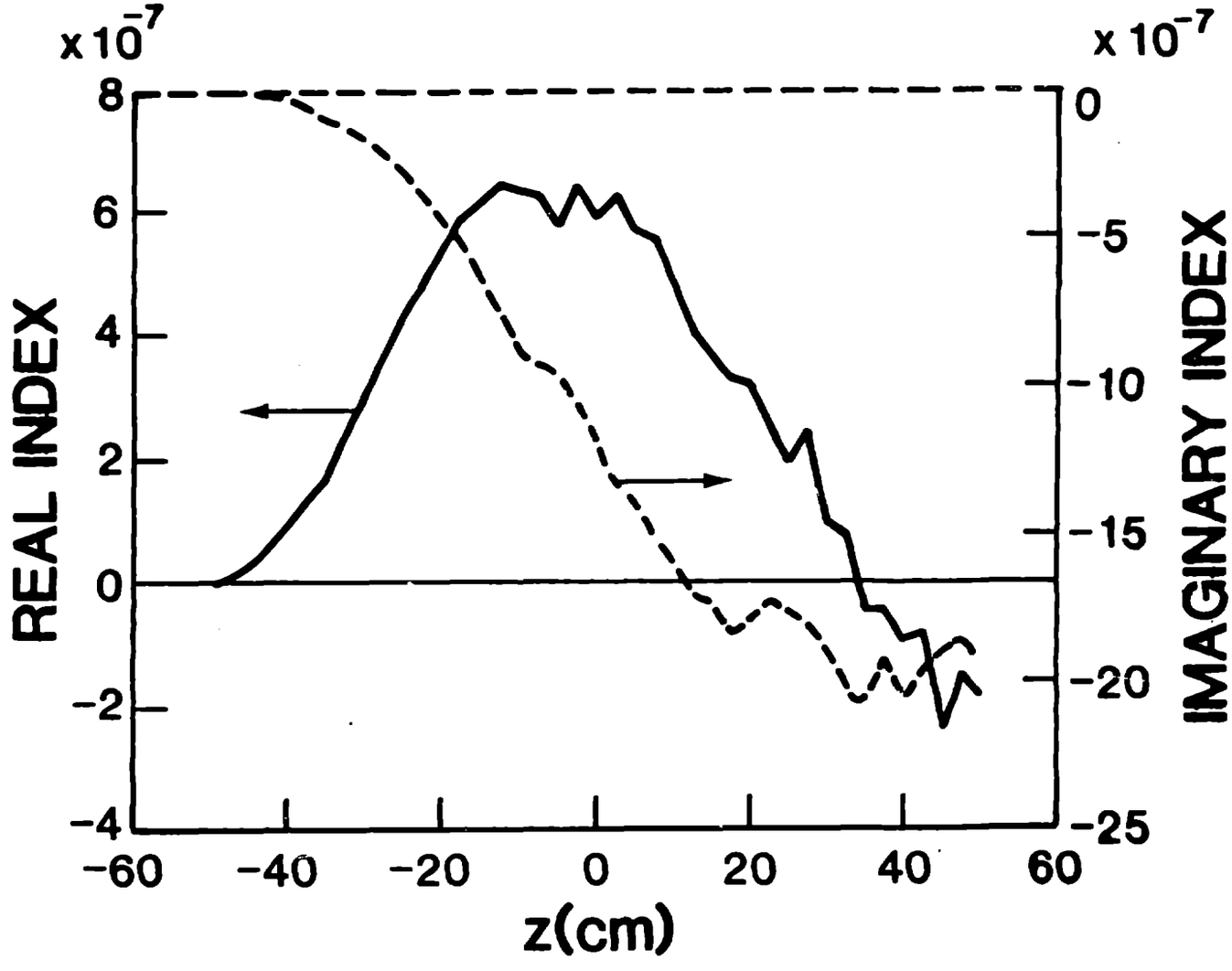


(SMALL SIGNAL)

Fig. 1b

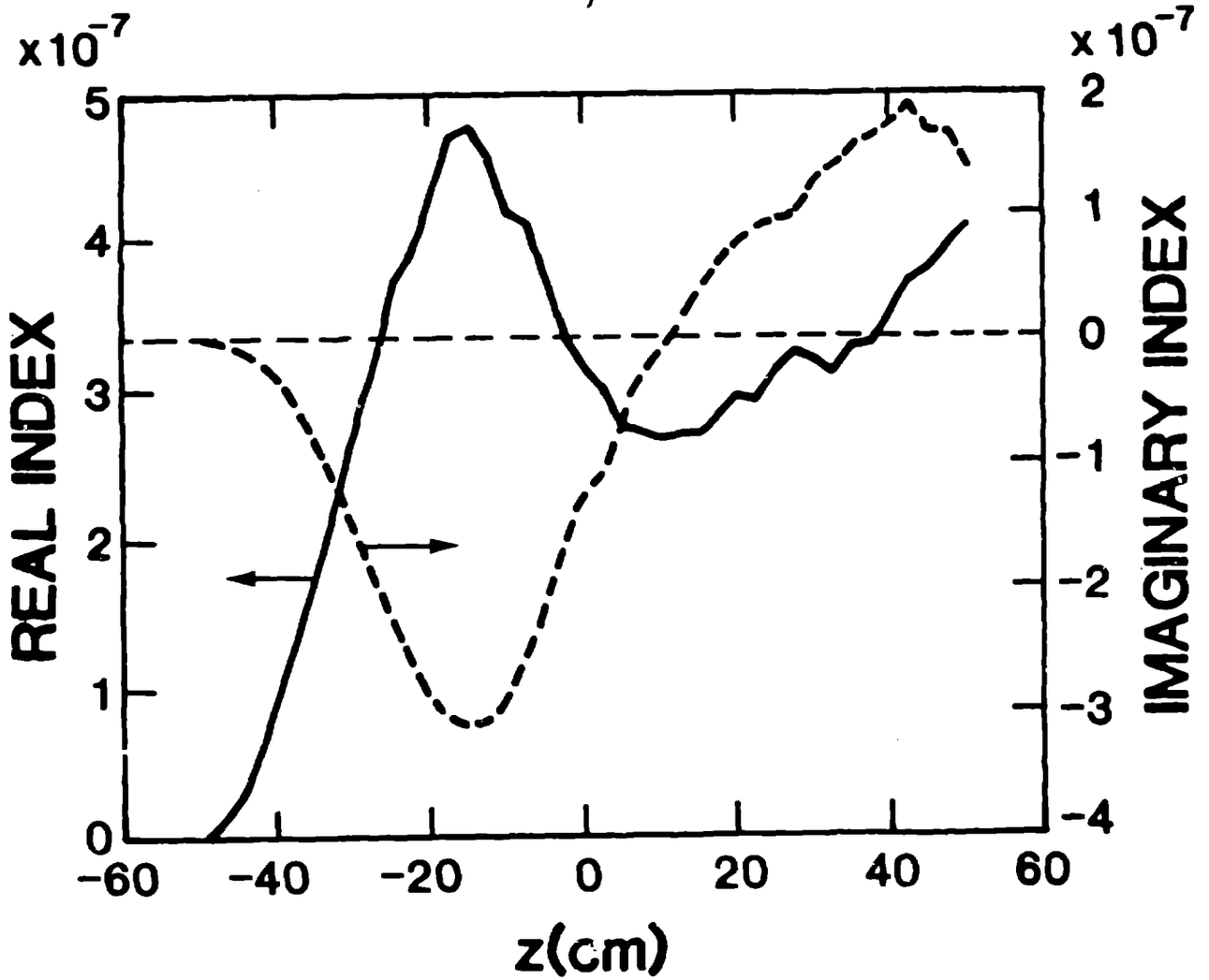


(SATURATED)

Fig. 2

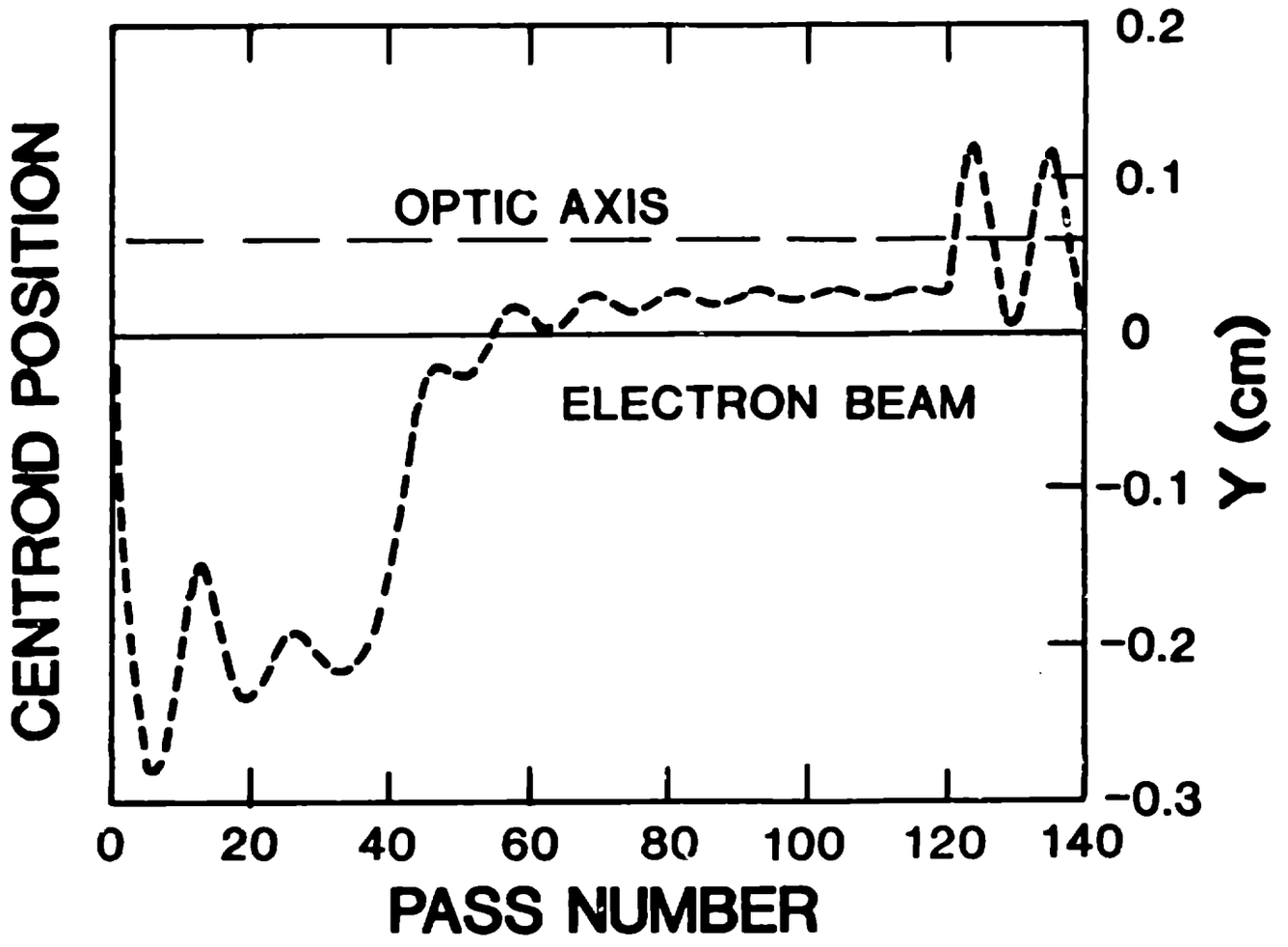
CENTROID POSITION
OPTIC AXIS
ELECTRON BEAM
0.2
0.1
0
−0.1
−0.2
−0.3
Y (cm)
0
20
40
60
80
100
120
140
PASS NUMBER

Fig. 3a

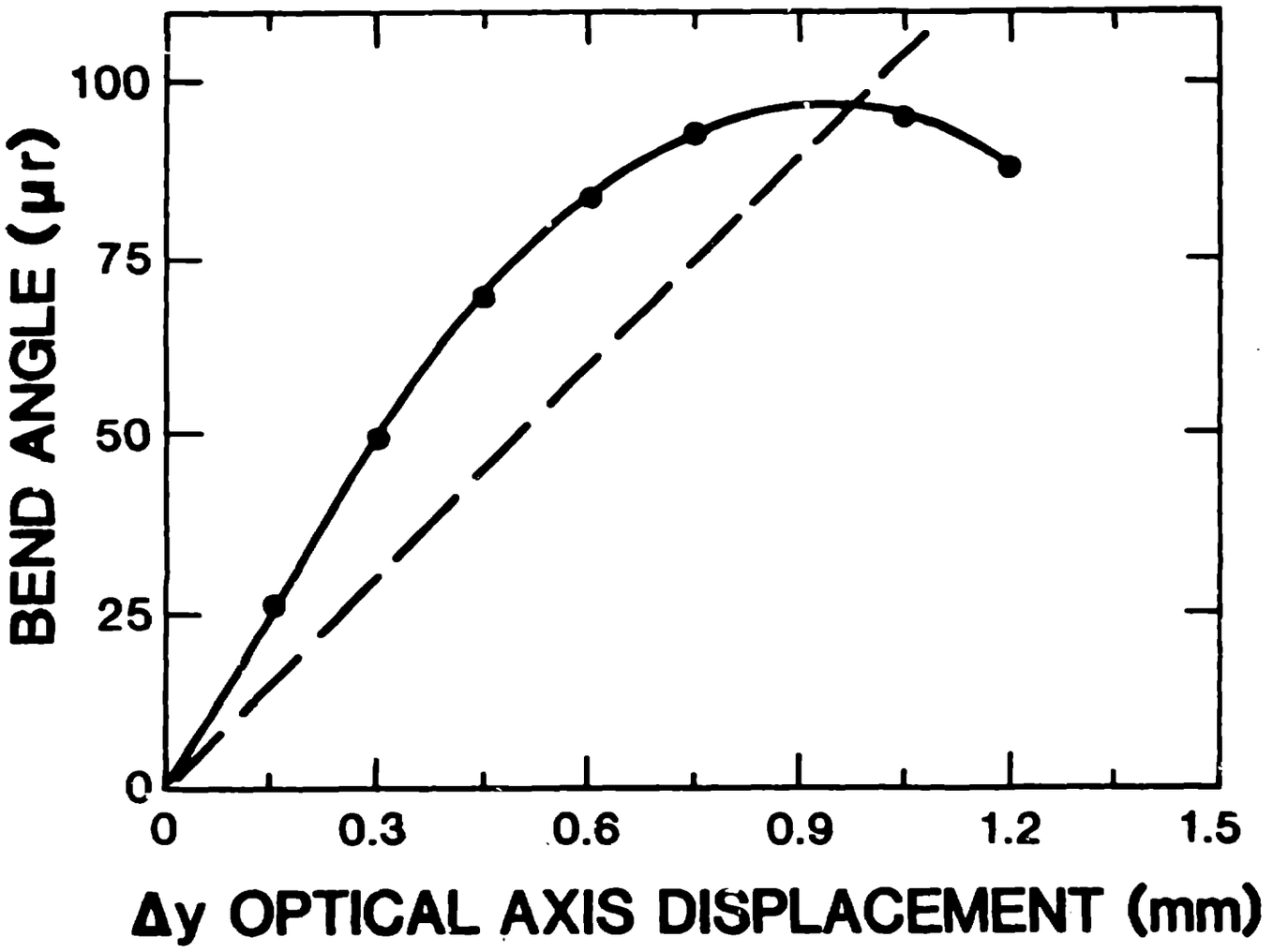
BEND ANGLE (μr)
100
75
50
25
0
0
0.3
0.6
0.9
1.2
1.5
Δy OPTICAL AXIS DISPLACEMENT (mm)

Fig. 3b

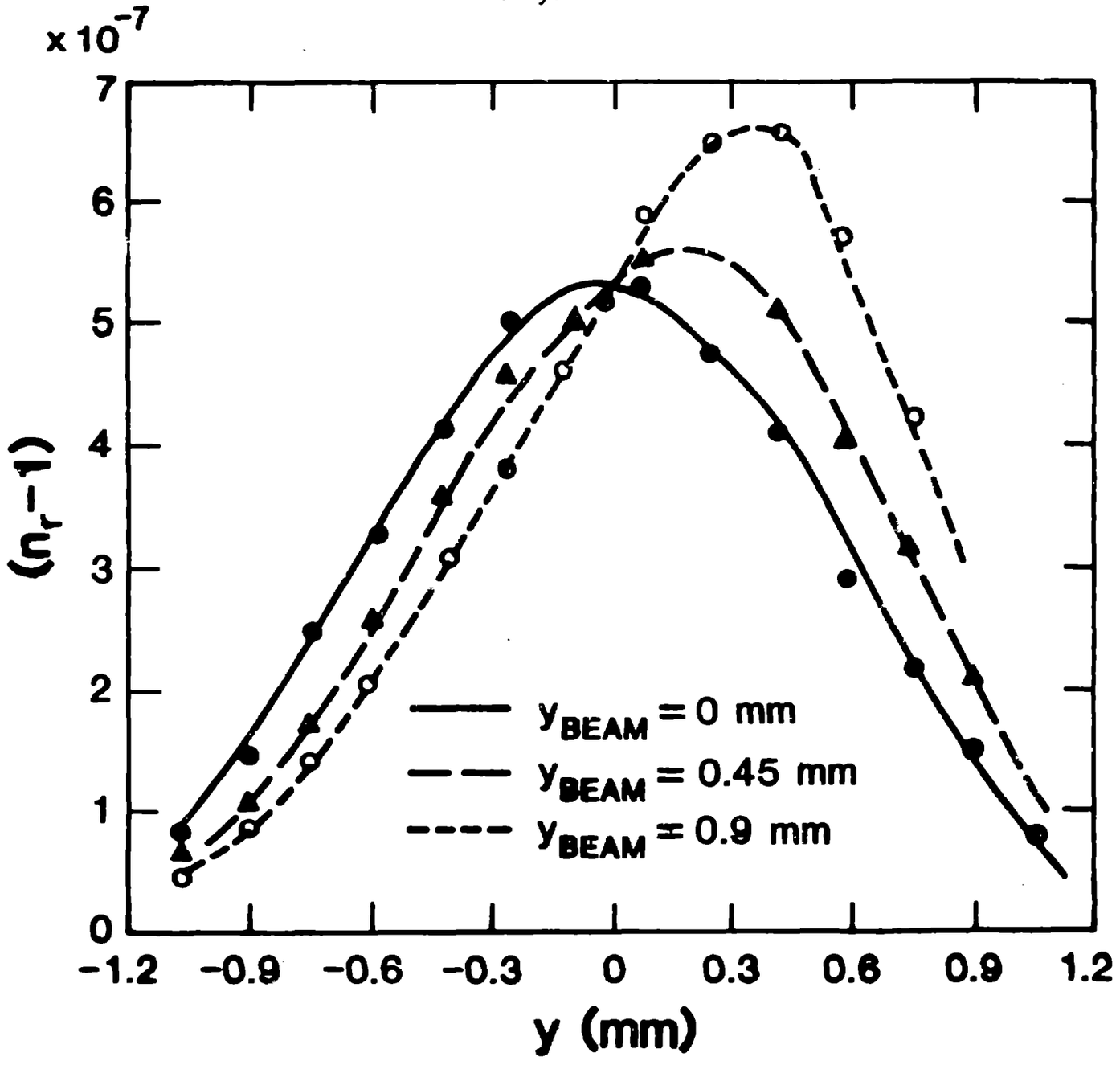
x 10^-7
7
6
5
4
3
2
1
0
(n_r − 1)
−1.2
−0.9
−0.6
−0.3
0
0.3
0.6
0.9
1.2
y (mm)
y_BEAM = 0 mm
y_BEAM = 0.45 mm
y_BEAM = 0.9 mm

Fig. 4a

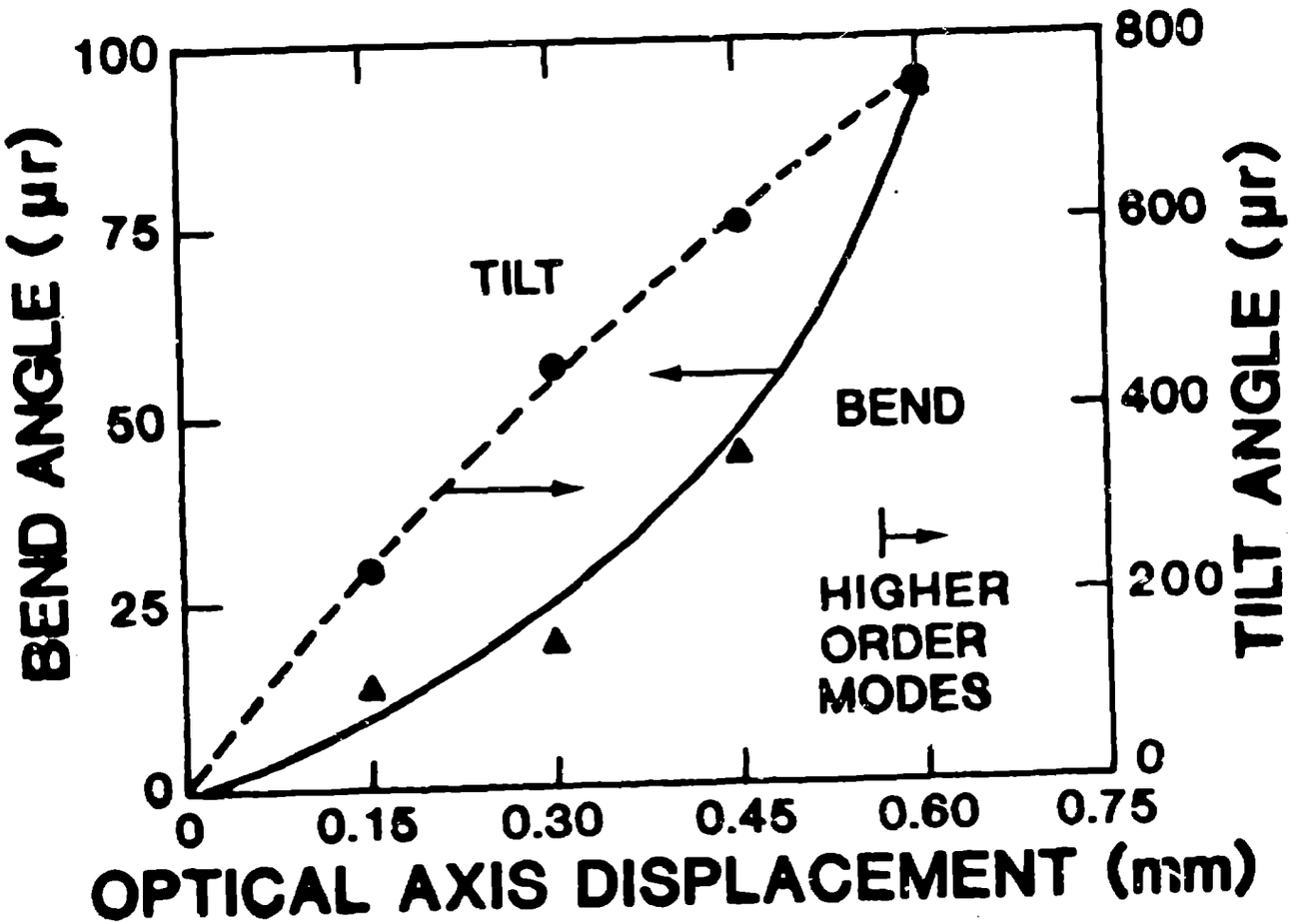
BEND ANGLE (μr)
TILT ANGLE (μr)
100
75
50
25
0
800
600
400
200
0
TILT
BEND
HIGHER
ORDER
MODES
0
0.15
0.30
0.45
0.60
0.75
OPTICAL AXIS DISPLACEMENT (mm)

Fig. 4b

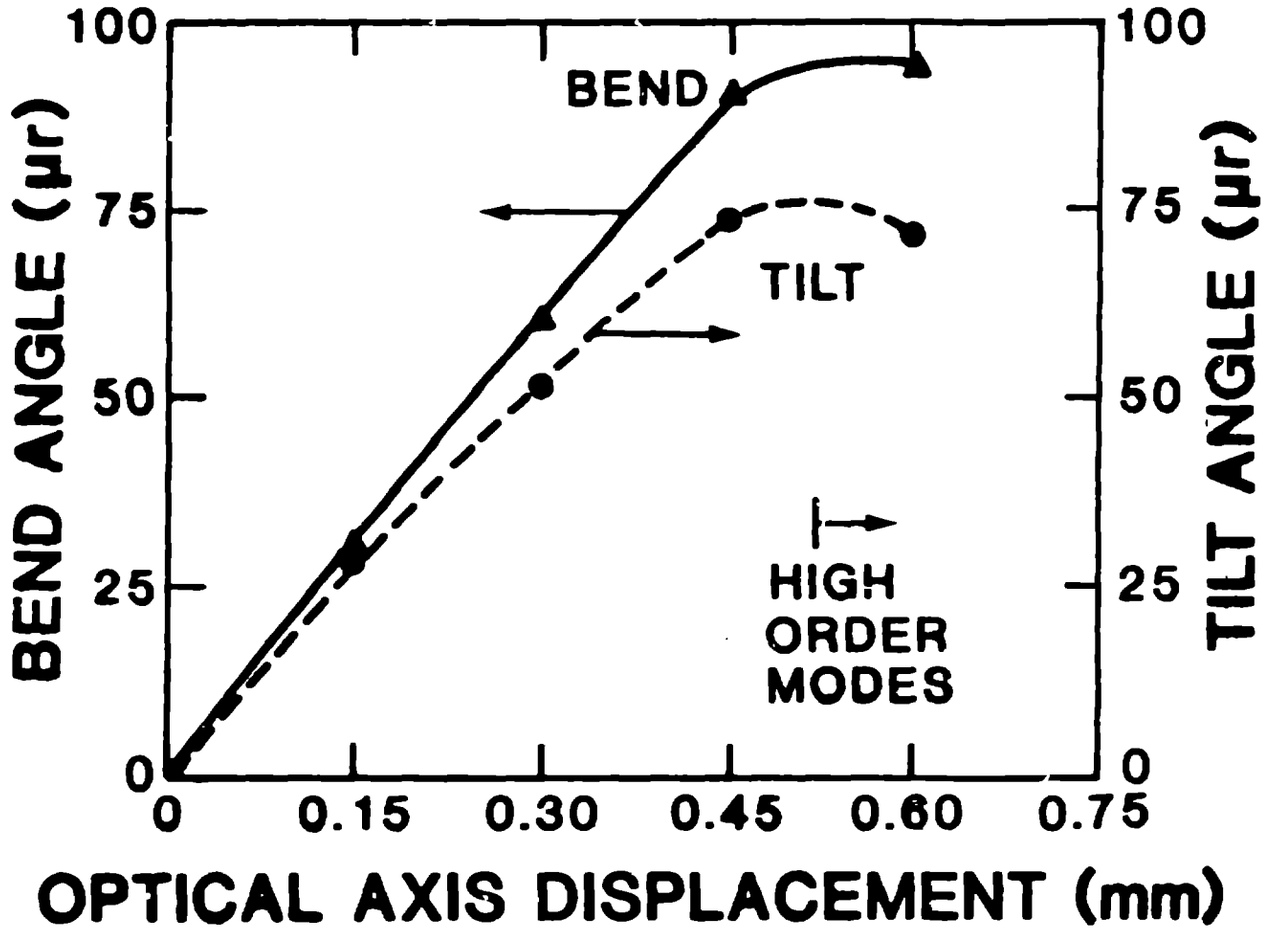
100
75
50
25
0
BEND ANGLE (μr)
BEND
TILT
HIGH
ORDER
MODES
100
75
50
25
0
TILT ANGLE (μr)
0
0.15
0.30
0.45
0.60
0.75
OPTICAL AXIS DISPLACEMENT (mm)

Fig. 5b

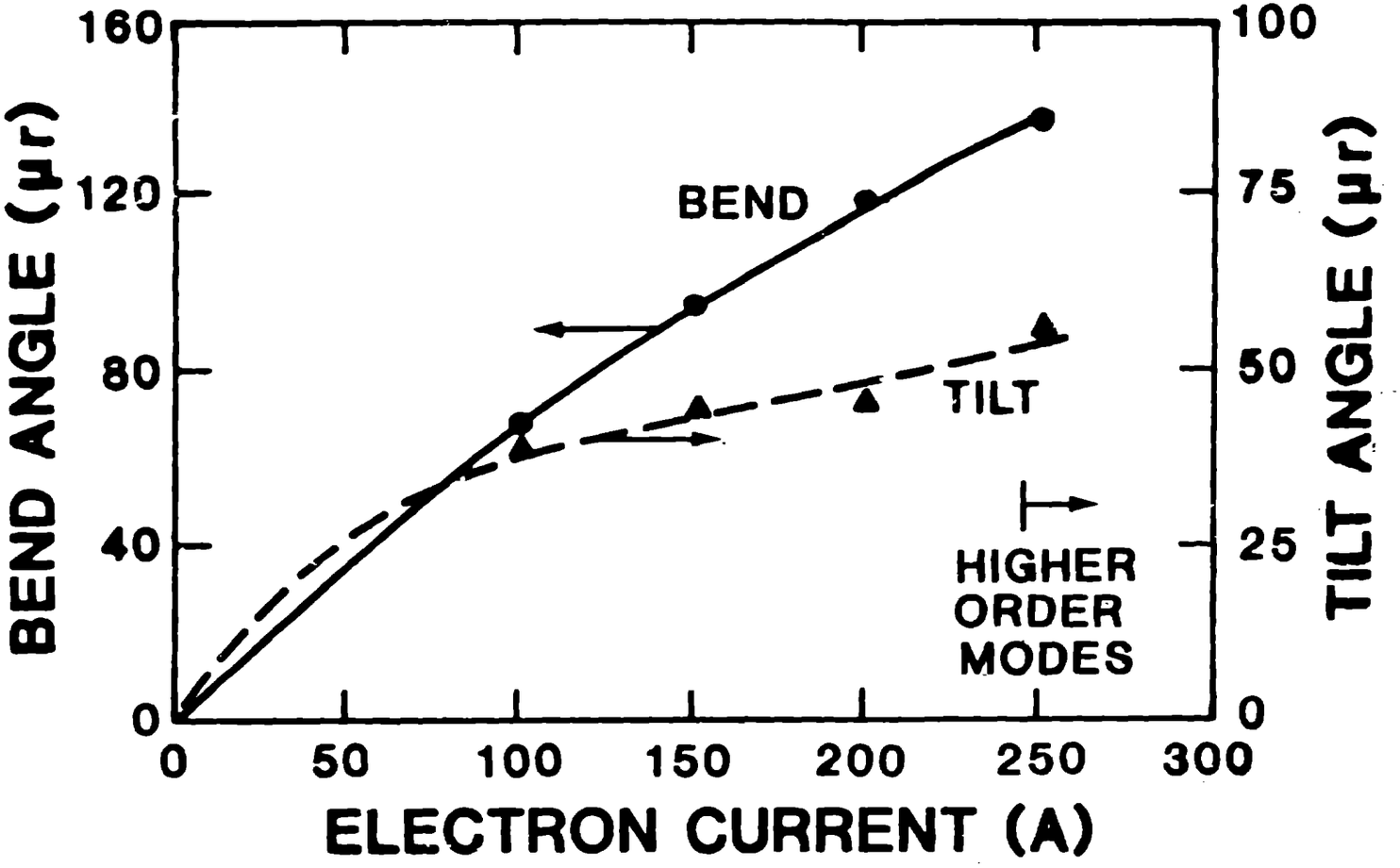
160
120
80
40
0
BEND ANGLE (μr)
100
75
50
25
0
TILT ANGLE (μr)
BEND
TILT
HIGHER
ORDER
MODES
0
50
100
150
200
250
300
ELECTRON CURRENT (A)

Fig. 5a

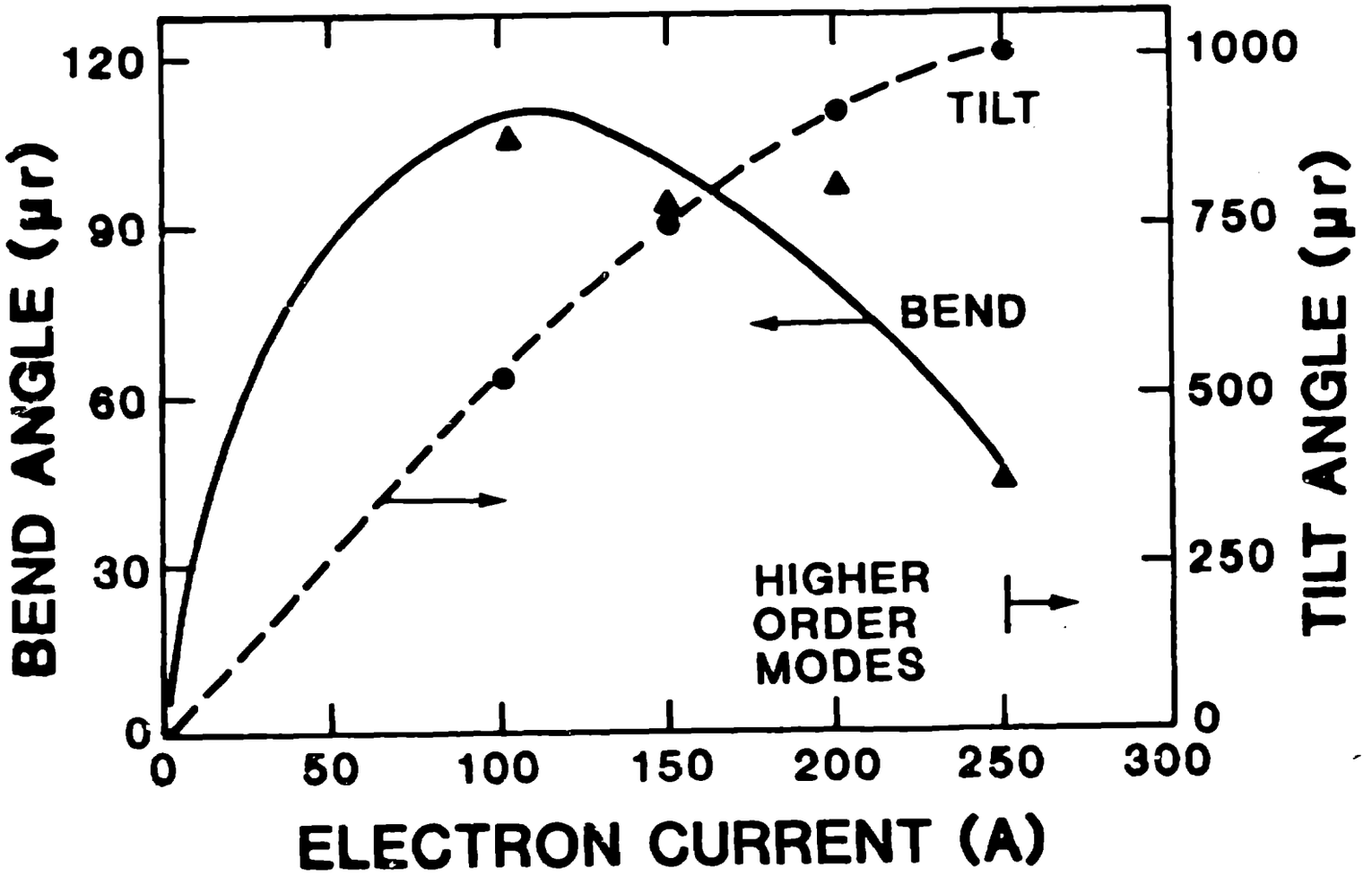
BEND ANGLE (μr)
TILT ANGLE (μr)
ELECTRON CURRENT (A)
TILT
BEND
HIGHER ORDER MODES
0
30
60
90
120
0
250
500
750
1000
0
50
100
150
200
250
300

Fig. 6

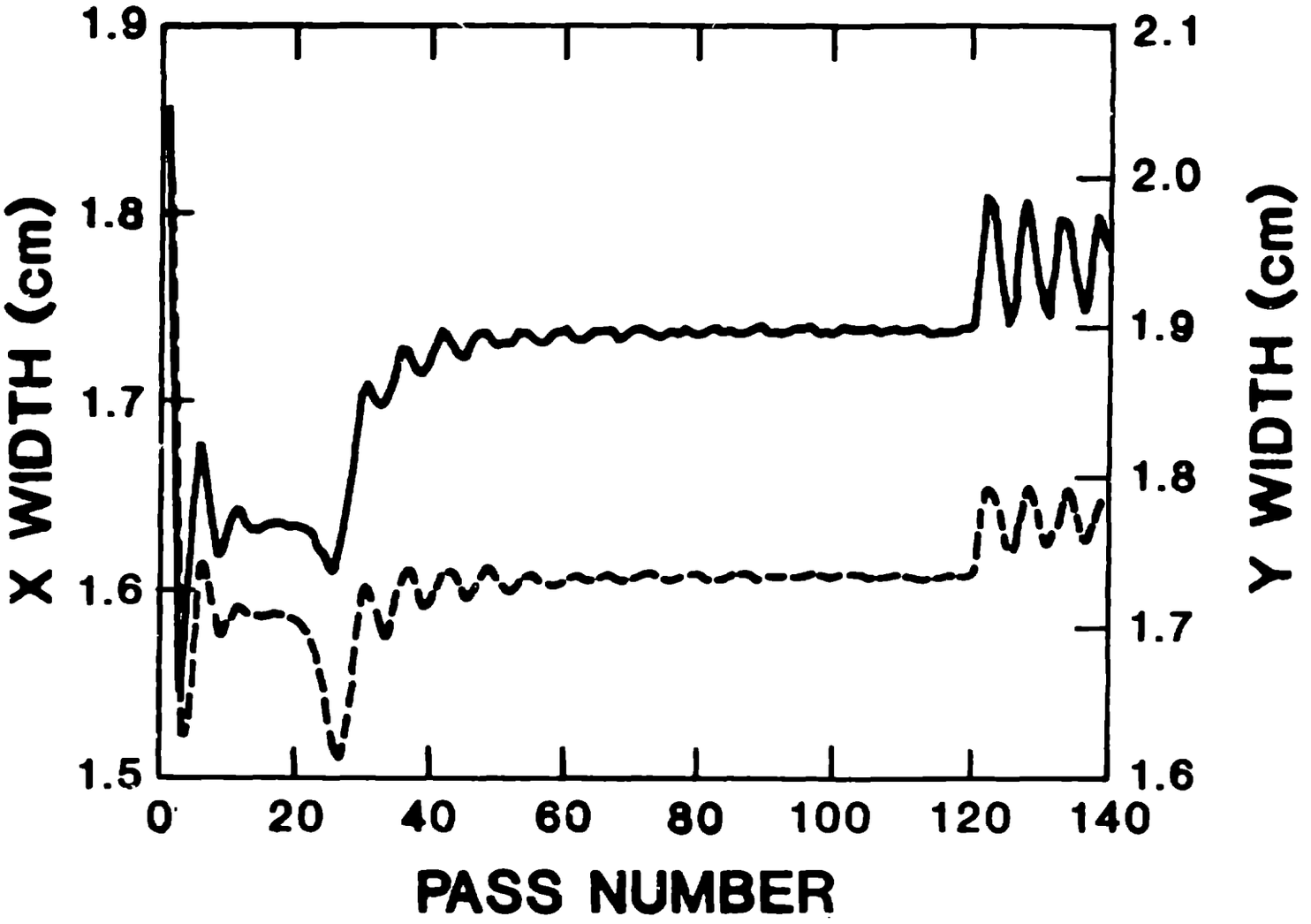
1.9
1.8
1.7
1.6
1.5
X WIDTH (cm)
2.1
2.0
1.9
1.8
1.7
1.6
Y WIDTH (cm)
0
20
40
60
80
100
120
140
PASS NUMBER

Fig. 7

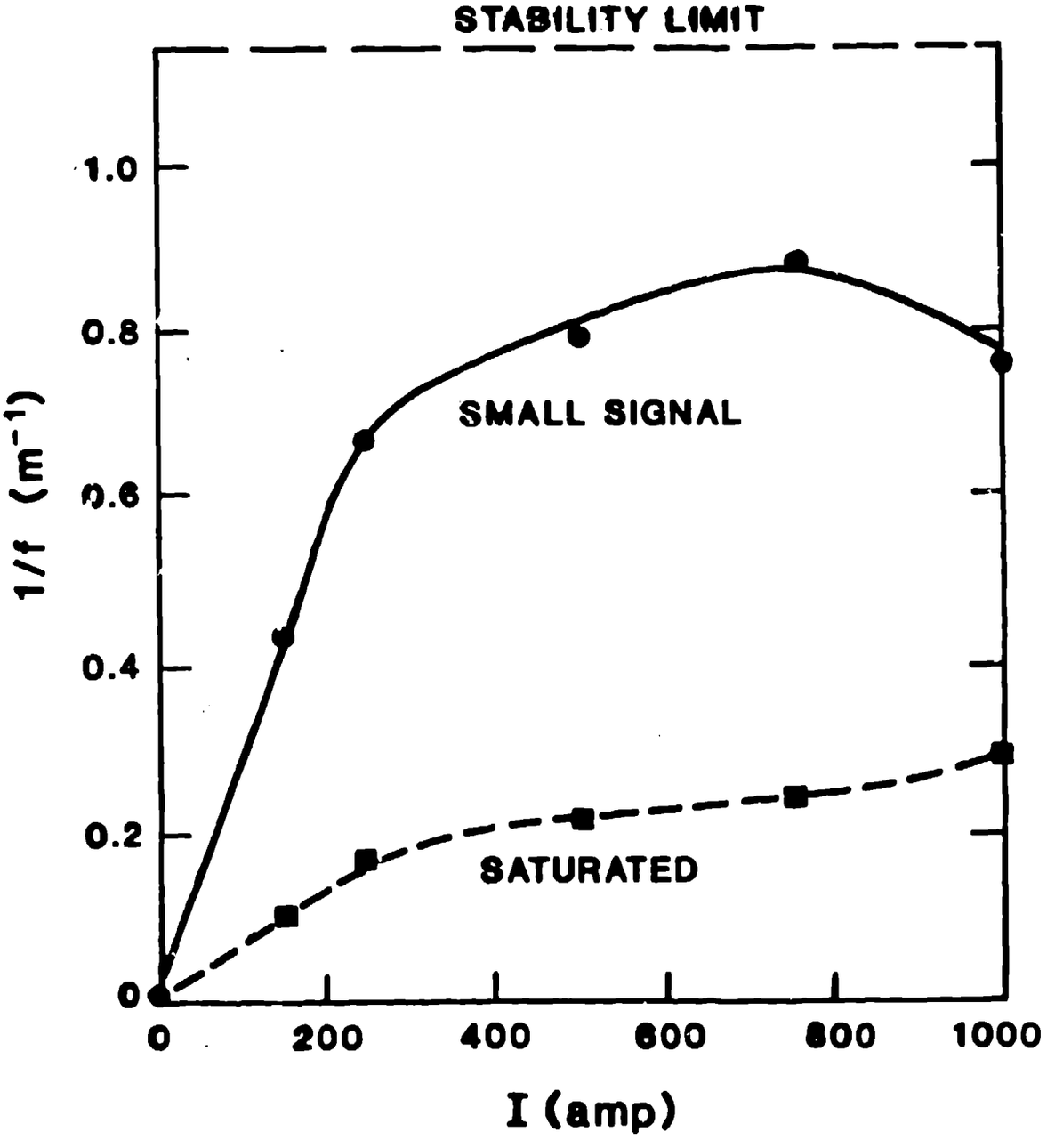
STABILITY LIMIT
1.0
0.8
0.6
0.4
0.2
0
1/f (m⁻¹)
SMALL SIGNAL
SATURATED
0
200
400
600
800
1000
I (amp)